

---

This is an electronic reprint of the original article.  
This reprint may differ from the original in pagination and typographic detail.

Cuesta, F. S.; Ptitsyn, G. A.; Mirmoosa, M. S.; Tretyakov, S. A.

## Coherent retroreflective metasurfaces

*Published in:*  
Physical Review Research

*DOI:*  
[10.1103/PhysRevResearch.3.L032025](https://doi.org/10.1103/PhysRevResearch.3.L032025)

Published: 01/09/2021

*Document Version*  
Publisher's PDF, also known as Version of record

*Published under the following license:*  
CC BY

*Please cite the original version:*  
Cuesta, F. S., Ptitsyn, G. A., Mirmoosa, M. S., & Tretyakov, S. A. (2021). Coherent retroreflective metasurfaces. *Physical Review Research*, 3(3), Article 032025. <https://doi.org/10.1103/PhysRevResearch.3.L032025>

---

This material is protected by copyright and other intellectual property rights, and duplication or sale of all or part of any of the repository collections is not permitted, except that material may be duplicated by you for your research use or educational purposes in electronic or print form. You must obtain permission for any other use. Electronic or print copies may not be offered, whether for sale or otherwise to anyone who is not an authorised user.

## Coherent retroreflective metasurfaces

F. S. Cuesta <sup>\*</sup>, G. A. Ptitcyn, M. S. Mirmoosa , and S. A. Tretyakov *Department of Electronics and Nanoengineering, Aalto University, P.O. Box 15500, FI-00076 Aalto, Finland*

(Received 22 December 2020; accepted 28 June 2021; published 30 July 2021)

Inhomogeneous metasurfaces have shown possibilities for unprecedented control of wave propagation and scattering. While it is conventional to shine a single incident plane wave from one side of these metastructures, illuminating by several waves simultaneously from both sides may enhance possibilities to control scattered waves, which results in additional functionalities and novel applications. Here, we unveil how by using coherent plane-wave illumination of a properly designed inhomogeneous metasurface sheet it is possible to realize controllable retroreflection. We call these metasurfaces “coherent retroreflectors” and explain the method for realizing them both in theory and in practice. We show that coherent retroreflectors can be used for filtering undesired modes and creation of field-localization regions in waveguides. The latter application is in resemblance to bound states in the radiation continuum.

DOI: [10.1103/PhysRevResearch.3.L032025](https://doi.org/10.1103/PhysRevResearch.3.L032025)

Metasurfaces, as optically thin layers structured at the subwavelength scale (e.g., [1–3]), introduce discontinuities for tangential components of electric and magnetic fields. We consider nonmagnetic layers with negligible thickness, which support exclusively electric surface currents. This condition limits possible functionalities as these metasurfaces only create a discontinuity of the magnetic field. For instance, homogeneous thin sheets of any material can absorb a maximum of 50% of the incident power of electromagnetic waves. However, this limitation is removed if both sides of the sheet are coherently illuminated, which can be achieved by positioning a reflector behind the sheet [4] or by illuminating the other side with a coherent wave [5,6] created by a splitter or an independent phase-locked generator. Similar observation can be made for fully reflective sheets. A single uniform sheet of negligible thickness can fully reflect incident waves only if it is perfectly conducting. Thus, there is no possibility to control reflection phase. This limitation can be also removed by adding a reflector behind the sheet, creating so-called high-impedance surfaces [7] or illuminating the two sides of the sheet by two coherent waves [8].

Despite these possibilities, homogeneous coherent metasurfaces cannot change the direction of propagation of incident waves. In contrast, optically thin sheets whose properties vary over the surface have this important capacity. In consequence, they can perform a multitude of functions, such as anomalous reflection, anomalous transmission, power splitting, focusing, surface-wave control, and so forth (e.g., [1]).

Nevertheless, similarly to uniform sheets, the functionalities of inhomogeneous sheets are also limited because the tangential electric field component still remains continuous across the sheet. Following an analogy with uniform coherent metasurfaces, we expect that coherent illuminations of surface-inhomogeneous sheets can dramatically widen the scope of controllable electromagnetic effects.

In this Letter, we propose surface-inhomogeneous coherent metasurfaces which can be defined as surface-varying sheets with extended properties under coherent illumination from both sides. In the literature, coherent illuminations of diffraction gratings (metagratings) have been studied [9–12]. Here, we discuss general space-periodical coherent metasurfaces. In particular, this Letter introduces and studies coherent metasurfaces designed for total retroreflection, as illustrated in Fig. 1.

Retroreflectors that are capable of reflecting the electromagnetic energy back to the source are essential for different important applications [13–20]. Similarly to the case of uniform sheets of negligible optical thickness, the performance of nonuniform sheets designed for retroreflection is fundamentally limited: they cannot reflect more than 25% of the incident power into the desired direction [21]. To dramatically enhance the efficiency, one can propose an elegant solution to use a *coherent* retroreflective sheet (as presented in Fig. 1) which can retroreflect completely the power from both sources.

We explain how to design coherent retroreflective metasurfaces for both transverse-electric (TE) and transverse-magnetic (TM) linearly polarized waves. Furthermore, we discuss how the proposed retroreflective metasurface can be effectively used to suppress unwanted waveguide modes and localize high-amplitude fields in unbounded waveguiding structures. In addition, we note that it is possible to replace conventional retroreflectors [20,22–29] with extremely light and thin coherent structures. Moreover, the coherent nature of retroreflection of the proposed structures also allows tunability, for instance, by turning the second wave on or off.

\*Corresponding author: francisco.cuestasoto@aalto.fi

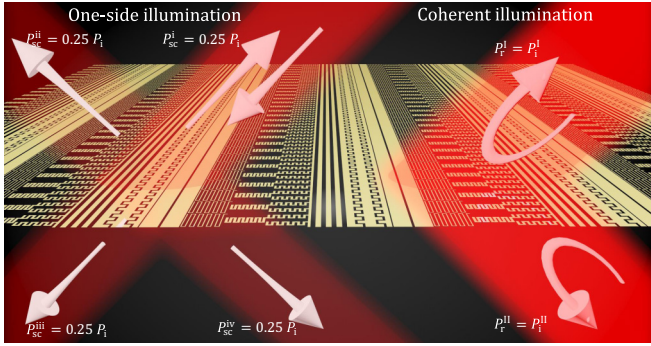


FIG. 1. A coherent retroreflective metasurface which is illuminated by two incident plane waves, from top and bottom, and reflects those incident waves fully in the same directions, without any parasitic additional modes.

Let us consider a metasurface sheet of negligible thickness as an interface between two vacuum regions, as shown in Fig. 2(a). We assume that the sheet supports only electric surface current, with the surface current density  $\mathbf{J}_s$ , and it is illuminated from both sides by plane waves with the incidence angle  $\theta_i$ . Such metasurface can be characterized by the boundary condition  $Z_s \mathbf{J}_s = (\mathbf{E}_{\tau,1} + \mathbf{E}_{\tau,2})/2$ , where  $\mathbf{E}_{\tau,1-2}$  ( $\mathbf{H}_{\tau,1-2}$ ) are the total tangential electric (magnetic) fields on the two sides of the metasurface, respectively, and  $Z_s$  denotes the corresponding surface impedance [30–32]. Here we assume that there is no cross-polarizing response. Since the tangential electric field is continuous across the sheet,  $\mathbf{E}_{\tau,1} = \mathbf{E}_{\tau,2} = \mathbf{E}_\tau$ , and the difference between the tangential magnetic field components is identical to the surface current density,  $\mathbf{n} \times (\mathbf{H}_{\tau,2} - \mathbf{H}_{\tau,1}) = -\mathbf{J}_s$  ( $\mathbf{n}$  is the unit vector orthogonal to the surface pointing into region 1), we can readily write that

$$\mathbf{n} \times (\mathbf{H}_{\tau,2} - \mathbf{H}_{\tau,1}) = -\frac{\mathbf{E}_\tau}{Z_s}. \quad (1)$$

In order to function as a retroreflector, the metasurface requires different surface impedance profiles depending on whether it is illuminated with TE or TM waves. In more detail, the desired field structure is a set of two incident plane waves,

which are illuminating the opposite sides of the metasurface, and two retroreflected plane waves. Let us first consider the TE polarization, illustrated in Fig. 2(a), in which case the fields are given by

$$\begin{aligned} \mathbf{E}_{I,1} &= E_{I,1} e^{-jk_0[\text{ysin}(\theta_i) - z\text{cos}(\theta_i)]} \mathbf{x}, \\ \mathbf{H}_{I,1} &= -\frac{E_{I,1}}{\eta_0} [\cos(\theta_i) \mathbf{y} + \sin(\theta_i) \mathbf{z}] e^{-jk_0[\text{ysin}(\theta_i) - z\text{cos}(\theta_i)]}, \\ \mathbf{E}_{R,1} &= E_{R,1} e^{jk_0[\text{ysin}(\theta_i) - z\text{cos}(\theta_i)]} \mathbf{x}, \\ \mathbf{H}_{R,1} &= \frac{E_{R,1}}{\eta_0} [\cos(\theta_i) \mathbf{y} + \sin(\theta_i) \mathbf{z}] e^{jk_0[\text{ysin}(\theta_i) - z\text{cos}(\theta_i)]}, \end{aligned} \quad (2)$$

in region 1, and

$$\begin{aligned} \mathbf{E}_{I,2} &= E_{I,2} e^{-jk_0[\text{ysin}(\theta_i) + z\text{cos}(\theta_i)]} \mathbf{x}, \\ \mathbf{H}_{I,2} &= \frac{E_{I,2}}{\eta_0} [\cos(\theta_i) \mathbf{y} - \sin(\theta_i) \mathbf{z}] e^{-jk_0[\text{ysin}(\theta_i) + z\text{cos}(\theta_i)]}, \\ \mathbf{E}_{R,2} &= E_{R,2} e^{jk_0[\text{ysin}(\theta_i) + z\text{cos}(\theta_i)]} \mathbf{x}, \\ \mathbf{H}_{R,2} &= \frac{E_{R,2}}{\eta_0} [-\cos(\theta_i) \mathbf{y} + \sin(\theta_i) \mathbf{z}] e^{jk_0[\text{ysin}(\theta_i) + z\text{cos}(\theta_i)]}, \end{aligned} \quad (4)$$

in region 2. Here,  $E_I$  and  $E_R$  represent the amplitudes of the incident and reflected waves, respectively. Also,  $\eta_0$  and  $k_0$  are the free-space intrinsic impedance and wave number. We consider the full-reflection scenario, where all the incident power is reflected by the metasurface, with reflected fields defined as  $E_{R,1} = E_{I,1} \exp(j\phi_{R,1})$  and  $E_{R,2} = E_{I,2} \exp(j\phi_{R,2})$ . In addition, we suppose that the incident electric fields have the same magnitude, but there is a difference in phase:  $E_{I,2} = E_{I,1} \exp(j\phi_{I,2})$ . Based on these considerations and Eqs. (2)–(5), we find the total tangential field components at the interface  $z = 0$  [21], impose the boundary conditions, and satisfy Eq. (1). This leads us to two important observations. First, total retroreflection is achieved only under coherent illumination with the same phase ( $\phi_{I,2} = 0$ ) and symmetric scattering ( $\phi_{R,1} = \phi_{R,2} = \phi_R$ ). Second, the surface impedance must have the following profile:

$$Z_s^{\text{TE}}(y) = j \frac{\eta_0}{2 \cos(\theta_i)} \cot \left( \frac{\phi_R}{2} + k_0 y \sin(\theta_i) \right). \quad (6)$$

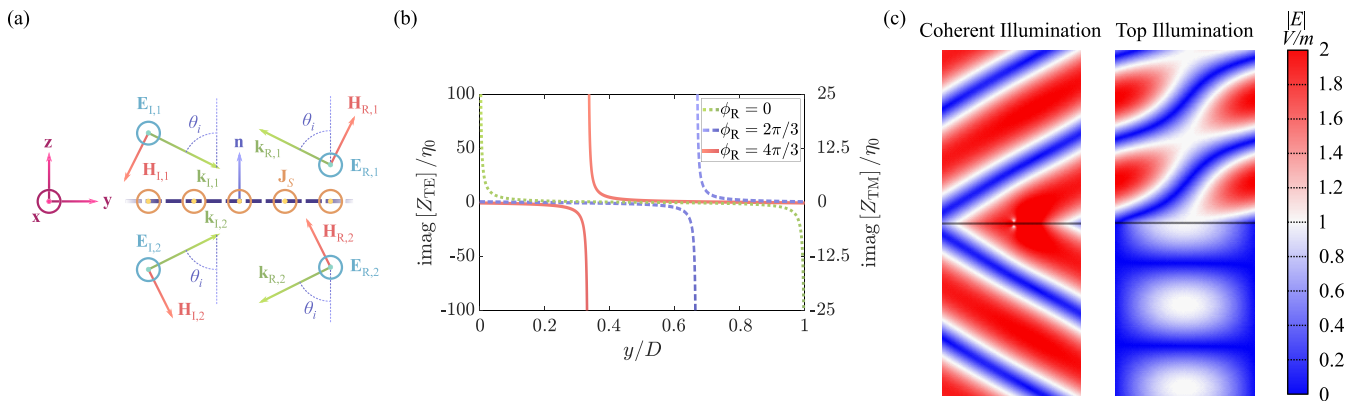


FIG. 2. (a) Schematic representation of a coherent retroreflector for TE waves. (b) Normalized reactance profile for TE- and TM-polarized coherent retroreflectors. The impedance for the two polarizations differ by the scale factor  $\cos(\theta_i)^2$  ( $\theta_i = 60^\circ$  for this illustration), using different values of  $\phi_R$ . (c) The coherent retroreflective sheet exhibits total retroreflection when it is illuminated from both sides; however, additional scattering is produced when it is illuminated from only one side ( $\theta_i = 60^\circ$ ,  $\phi_R = 0^\circ$ , and  $f = 10$  GHz for this illustration).

Thus, the surface impedance of coherent retroreflective sheets for TE polarization is a function of the position with the period  $D = \lambda_0/[2 \sin(\theta_i)]$  which depends on the angle of incidence and frequency (recall that  $k_0 = 2\pi/\lambda_0$ ). It is worth mentioning that the effect of the reflection phase on the surface impedance is equivalent to a displacement of the retroreflective sheet along the  $y$  axis, as portrayed in Fig. 2(b). Simulation results, presented in Fig. 2(c), demonstrate that total retroreflection is achieved when the sheet is illuminated from both sides, while additional waves are scattered when it is illuminated from only one side.

The required surface impedance for TM polarization can be found by similar means [21], and it reads

$$Z_s^{\text{TM}}(y) = j \frac{\eta_0 \cos(\theta_i)}{2} \cot\left(\frac{\phi_R}{2} + k_0 y \sin(\theta_i)\right). \quad (7)$$

As is seen from the above two equations, surface impedances for TM and TE polarizations are quite similar, with the cosine term as the only difference. Note that this impedance differs only by the factor 1/2 from the sheet impedance of free-space retroreflectors formed by an inhomogeneous reactive sheet over a uniform mirror (e.g., [20,33]). Thus, the same design formulas and the same designed metasurface topologies can be used also to create free-space coherent retroreflectors.

To illustrate the capabilities of surface-inhomogeneous coherent metasurfaces, we suggest two relevant applications where thin sheets can be effectively employed as coherent retroreflectors. The first application is about filtering undesired waveguide modes. We consider a parallel-plate waveguide which is formed by two ideally conducting sheets, as shown in Fig. 3(a). The TM or TE modes propagating inside a parallel-plate waveguide can be expressed as superpositions of two plane waves having opposite components of the wave vector (the components that are perpendicular to the phase front) (e.g., Refs. [34]). Due to this crucial property, a coherent retroreflective metasurface, illuminated by these two plane waves, is able to prevent the propagation of a specific mode without disturbing the other modes. To realize this functionality, we need to position the metasurface in the middle of the waveguide, between the two boundaries, and choose the corresponding surface impedance properly. In practical realizations, the metasurface consists of a highly conductive pattern over a dielectric substrate. In the design of coherent metasurfaces, the patterned layer should be placed in the middle of the substrate in order to preserve symmetry. For the considered application, it is preferable to use low-permittivity substrates and small thickness, to minimize interference with other modes [21]. Alternatively, the whole waveguide can be filled with an isotropic dielectric material such as glass or polymer, which provides the necessary mechanical support for the metasurface without creating discontinuities in the waveguide cross section. In this case the effect of the host media needs to be accounted for in Eqs. (6) and (7).

As a proof-of-concept example, let us assume that the waveguide has  $h = 33.31$  mm distance between the plates, enough to allow free propagation of transverse-electromagnetic (TEM),  $\text{TE}_1$ , and  $\text{TM}_1$  modes at the reference frequency of  $f_0 = 10$  GHz, even in the scenario when a thin perfect electric conductor (PEC) plate is placed in the middle of the waveguide. Suppose that the  $\text{TM}_1$  mode is undesired,

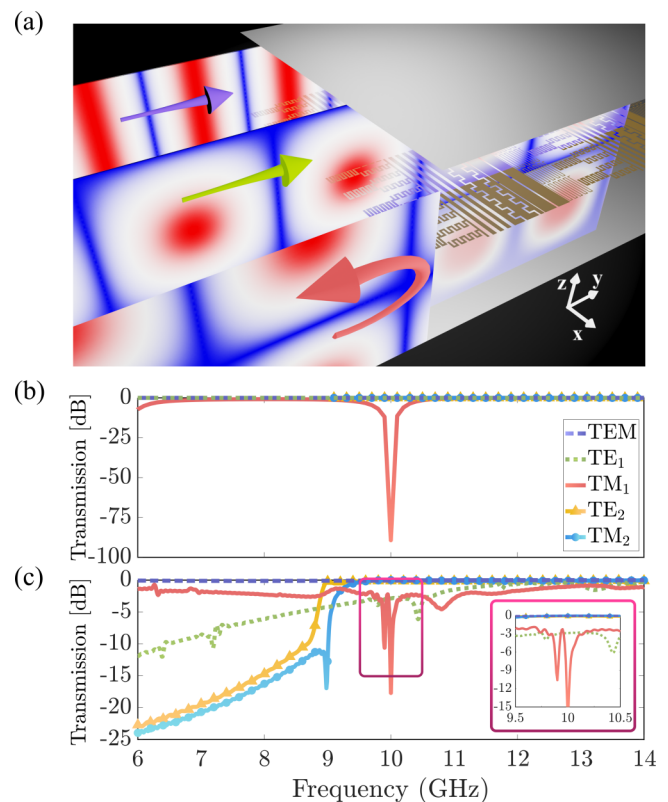


FIG. 3. (a) A parallel-plate waveguide which allows propagation of TEM,  $\text{TE}_1$ , and  $\text{TM}_1$  modes. However, a coherent retroreflective sheet placed between the plates acts as a mode filter, preventing propagation of a given mode ( $\text{TM}_1$  mode in this proof-of-concept example). (b) and (c) Simulation results for a coherent retroreflective metasurface reveal that  $\text{TM}_1$  can be suppressed at 10 GHz, without affecting propagation of other modes for (b) using six-discretized surface impedance stripes in COMSOL MULTIPHYSICS and (c) a metasurface implementation based on meandered slots and dipoles in CST MICROWAVE STUDIO [21]. Note that the COMSOL results are available only for frequencies greater than the mode cutoff frequency: 4.5 GHz for  $\text{TE}_1$  and  $\text{TM}_1$  modes; and 9 GHz for  $\text{TE}_2$  and  $\text{TM}_2$  modes.

and, therefore, we are interested in blocking this specific mode. Since the angle of incidence for each mode is given by  $\theta_i = \arccos[n\lambda_0/(2h)]$  in which  $\lambda_0$  is the wavelength and  $n$  represents the mode number [34], we simply calculate the required surface impedance in accordance with Eq. (7) and the  $\text{TM}_1$  mode. To see if such designed metasurface prevents the propagation of the undesired mode, we do numerical simulations using COMSOL MULTIPHYSICS software. Figure 3(b) shows numerical results where the transmittance and reflectance of the three modes have been observed in the case when the designed coherent retroreflective metasurface, realized as six surface-impedance stripes [20] with a total length of  $l = 17.73$  mm (one period  $D$ ), reference reflection phase  $\phi_R = 41.85^\circ$ , and incident angle  $\theta_i = 57.72^\circ$ , is placed in the middle of the waveguide. As seen, while the transmission of the TEM and  $\text{TE}_1$  modes is not influenced by the presence of the metasurface over a large bandwidth, the  $\text{TM}_1$  mode is effectively blocked by the metasurface at the design frequency. This simulation was also performed for higher-order modes,  $\text{TE}_2$  and  $\text{TM}_2$ , and we observed that the correspond-

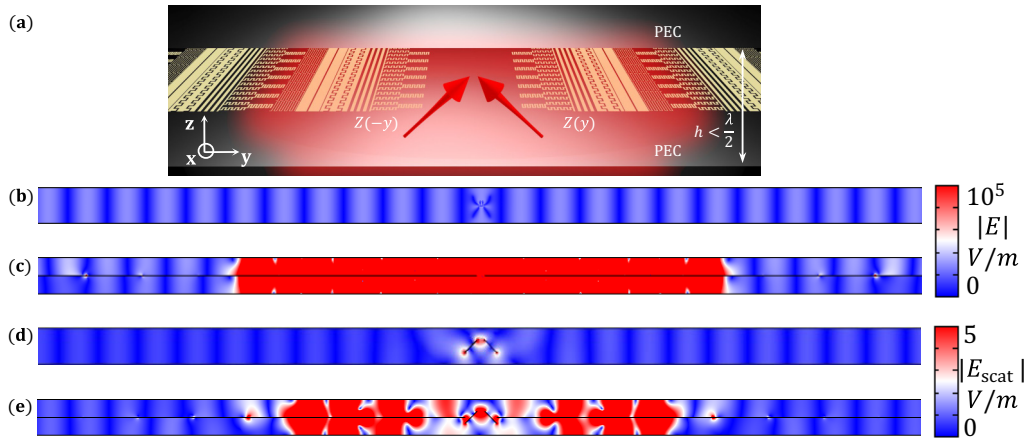


FIG. 4. (a) Schematic of a geometry using two retroreflectors for field localization. (b) and (c) Electric field amplitude created by two sources inside a waveguide without a metasurface in (b) and with a metasurface in (c). (d) and (e) Scattered electric field amplitude of waves created by a plane wave inside a waveguide without a metasurface in (d) and with a metasurface in (e). The separation distance between the centers of wire scatterers is  $\lambda_0/4$ , and the operational frequency in all simulations is 10 GHz.

ing transmission of those modes remains unchanged with the presence of the metasurface, as expected. Similar results were obtained for the conceptual design shown in Fig. 3(a) [21,35], where simulations carried in CST MICROWAVE STUDIO show that the  $TM_1$  mode was attenuated close to 20 dB at 10 GHz without affecting TEM,  $TE_2$ , and  $TM_2$  modes, as portrayed in Fig. 3(c). However, the  $TE_1$  mode is affected by the near fields scattered by the meta-atoms, rather than by the surface impedance profile itself, being attenuated around 3 dB at 10 GHz. This issue can be mitigated by using meta-atoms with smaller dimensions, resulting in more homogeneous surface impedances.

The second application is based on the use of coherent retroreflectors inside a waveguide to achieve significant field localization. A pair of coherent retroreflectors is aligned as shown in Fig. 4(a). The surface impedance profile of one metasurface is mirrored with respect to the other one, so that both metasurfaces reflect back to the center of the structure. In this arrangement, some energy emitted by a small source positioned in the center is trapped in the source vicinity as in a resonator, although there is no physical boundary in the waveguide. In order to demonstrate this concept, let us consider a narrow ( $h < \lambda_0/2$ ) parallel-plate waveguide, such that only the TEM mode is supported. First, we position two Hertzian dipole sources oriented as shown in Fig. 4(a) inside an empty waveguide, without the metasurfaces. In order to excite waves with a nonzero  $y$  component of electric field, the dipoles are separated by a small distance  $\delta \sim 0.025\lambda_0$ . In the waveguide without retroreflective sheets, the dipoles excite TEM waves which propagate away from the sources, as illustrated in Fig. 4(b). However, the addition of two coherent retroreflectors creates a significant field-localization region, as seen in Fig. 4(c). The result is obtained for the retroreflection phase  $\phi_R = 343^\circ$ . Since the metasurfaces are infinitely thin, they do not interact with the TEM wave propagating along the  $y$  direction, and we see that outside of the field-localization region the field is close to that of a single TEM mode.

Similar field-localization effects can be achieved in the scattering regime. To demonstrate that, we remove the Hertzian dipole sources and position two small PEC wire scatterers at the center of the structure. The waveguide is excited by a wave port at the left end of the simulation domain. The two PEC wires are rotated at the angle  $\pm 45^\circ$  and separated by  $\lambda_0/4$  distance, so that they excite enough strong electric fields with the  $y$  component in the vicinity of the scatterers [see Fig. 4(d)]. We need two wire scatterers in order to create two coherent scattered waves, equal in amplitude. Simulations confirm that placing metasurfaces around the wire scatterers enables us to trap a significant portion of the scattered energy in the vicinity of the scatterers. Figure 4(e) demonstrates localization of the scattered fields when the metasurface is inserted inside the waveguide. This result is achieved using the reflection phase  $\phi_R = 305^\circ$ . It is important to note that localization takes place without any physical boundary separating the volume of the “virtual resonator” from the rest of the waveguide. In these setups, the metasurfaces extend over the whole length of the waveguide. This property resembles bound states in the continuum, because the localization domain is fully open to both ends of the waveguide. In this case the length of the localization domain and the field enhancement level are determined by the designed angle of retroreflection. In the case when the metasurface is cut, the size of the field localization spot can be reduced and the field enhancement can be further boosted by rotating the source dipoles and properly redesigning the metasurface [21].

In summary, we propounded the concept of coherent surface-inhomogeneous metasurfaces on an example of retroreflective sheets, whose attribute is to reflect plane waves back to the source when they are illuminated from both sides simultaneously. Unlike retroreflective boundaries, the proposed coherent retroreflective sheet reaches total retroreflection without the use of additional layers. This work presented scenarios of practical applications of non-homogeneous surfaces under coherent illumination. Through

electromagnetic simulations, we have developed coherent retroreflective sheets that are capable to prevent propagation of a given electromagnetic mode in a multimode waveguide, without interfering with other modes; and to create localized field regions inside waveguides. The latter one can be viewed as an alternative approach for realization of bound states in

the radiation continuum. We expect that extending the concept of coherent inhomogeneous sheets to other metasurface functionalities will reveal other interesting new phenomena.

This work was supported in part by the Academy of Finland under grant 330260.

- 
- [1] S. B. Glybovski, S. A. Tretyakov, P. A. Belov, Y. S. Kivshar, and C. R. Simovski, Metasurfaces: From microwaves to visible, *Phys. Rep.* **634**, 1 (2016).
- [2] N. Yu and F. Capasso, Flat optics with designer metasurfaces, *Nat. Mater.* **13**, 139 (2014).
- [3] L. Zhang, S. Mei, K. Huang, and C.-W. Qiu, Advances in full control of electromagnetic waves with metasurfaces, *Adv. Opt. Mater.* **4**, 818 (2016).
- [4] Y. Radi, C. R. Simovski, and S. A. Tretyakov, Thin Perfect Absorbers for Electromagnetic Waves: Theory, Design, and Realizations, *Phys. Rev. Appl.* **3**, 037001 (2015).
- [5] D. G. Baranov, A. Krasnok, T. Shegai, A. Alù, and Y. Chong, Coherent perfect absorbers: Linear control of light with light, *Nat. Rev. Mater.* **2**, 17064 (2017).
- [6] S. Li, J. Luo, S. Anwar, S. Li, W. Lu, Z. H. Hang, Y. Lai, B. Hou, M. Shen, and C. Wang, Broadband perfect absorption of ultrathin conductive films with coherent illumination: Superabsorption of microwave radiation, *Phys. Rev. B* **91**, 220301(R) (2015).
- [7] D. Sievenpiper, L. Zhang, R. Broas, N. Alexopolous, and E. Yablonovitch, High-impedance electromagnetic surfaces with a forbidden frequency band, *IEEE Trans. Microwave Theory Tech.* **47**, 2059 (1999).
- [8] X. Fang, K. F. MacDonald, and N. I. Zheludev, Controlling light with light using coherent metadevices: All-optical transistor, summator and inverter, *Light: Sci. Appl.* **4**, e292 (2015).
- [9] Z. Zhang, M. Kang, X. Zhang, X. Feng, Y. Xu, X. Chen, H. Zhang, Q. Xu, Z. Tian, W. Zhang, A. Krasnok, J. Han, and A. Alù, Coherent perfect diffraction in metagratings, *Adv. Mater.* **32**, 2002341 (2020).
- [10] K. Achouri, G. Lavigne, M. A. Salem, and C. Caloz, Metasurface spatial processor for electromagnetic remote control, *IEEE Trans. Antennas Propag.* **64**, 1759 (2016).
- [11] J. Shi, X. Fang, E. T. F. Rogers, E. Plum, K. F. MacDonald, and N. I. Zheludev, Coherent control of Snell's law at metasurfaces, *Opt. Express* **22**, 21051 (2014).
- [12] F. He, K. F. MacDonald, and X. Fang, Continuous beam steering by coherent light-by-light control of dielectric metasurface phase gradient, *Opt. Express* **28**, 30107 (2020).
- [13] T. Takatsuji, M. Goto, S. Osawa, R. Yin, and T. Kurosawa, Whole-viewing-angle cat's-eye retroreflector as a target of laser trackers, *Meas. Sci. Technol.* **10**, N87 (1999).
- [14] S. P. Griggs, M. B. Mark, and B. J. Feldman, Dynamic optical tags, in *Battlespace Digitization and Network-Centric Systems IV*, edited by R. Suresh, International Society for Optics and Photonics (SPIE, Bellingham, WA, 2004), Vol. 5441, pp. 151–160.
- [15] G. C. Gilbreath, W. S. Rabinovich, T. J. Meehan, M. J. Vilcheck, R. Mahon, R. Burris, M. F. Stell, I. Sokolsky, J. A. Vasquez, C. S. Bovais, K. Cochrell, K. C. Goins, R. Barbehenn, D. S. Katzer, K. Ikossi-Anastasiou, and M. J. Montes, Large-aperture multiple quantum well modulating retroreflector for free-space optical data transfer on unmanned aerial vehicles, *Opt. Eng.* **40**, 1348 (2001).
- [16] L. Zhou, J. M. Kahn, and K. S. J. Pister, Corner-cube retroreflectors based on structure-assisted assembly for free-space optical communication, *J. Microelectromech. Syst.* **12**, 233 (2003).
- [17] W. S. Rabinovich, R. Mahon, P. G. Goetz, E. Waluschka, D. S. Katzer, S. C. Binari, and G. C. Gilbreath, A cat's eye multiple quantum-well modulating retro-reflector, *IEEE Photon. Technol. Lett.* **15**, 461 (2003).
- [18] B. A. Warneke, M. D. Scott, B. S. Leibowitz, Lixia Zhou, C. L. Bellew, J. A. Chediak, J. M. Kahn, B. E. Boser, and K. S. J. Pister, An autonomous 16 mm/sup 3/solar-powered node for distributed wireless sensor networks, in *Proceedings of the 2002 IEEE SENSORS* (IEEE, New York, 2002), Vol. 2, pp. 1510–1515.
- [19] K. Ozawa, N. Koga, N. Sugimoto, Y. Saito, A. Nomura, T. Aoki, T. Itabe, and H. Kunimori, Laser transmitter/receiver system for earth-satellite-earth long-path absorption measurements of atmospheric trace species using the retroreflector in space, *Opt. Eng.* **36**, 3235 (1997).
- [20] F. S. Cuesta, V. A. Lenets, A. Díaz-Rubio, A. Khripkov, and S. A. Tretyakov, Metasurface retroreflector for controlling parasitic surface waves on waves on bodies of 5G mobile phones, [arXiv:2008.12542](https://arxiv.org/abs/2008.12542).
- [21] See Supplemental Material at <http://link.aps.org/supplemental/10.1103/PhysRevResearch.3.L032025> for complete derivation of equations found in this letter, metasurface design, discussion of the effect of small-volume field localization, and additional insights related with performance under different illumination angles and frequencies.
- [22] K. V. Acoleyen, D. C. O'Brien, F. Payne, W. Bogaerts, and R. Baets, Optical retroreflective marker fabricated on silicon-on-insulator, *IEEE Photon. J.* **3**, 789 (2011).
- [23] T. Nagayama, S. Fukushima, A. Sanada, and T. Watanabe, Flat retroreflector based on transformation electromagnetics, in *Proceedings of the 2016 International Conference on Advanced Technologies for Communications (ATC)* (IEEE, New York, 2016).
- [24] A. M. H. Wong, P. Christian, and G. V. Eleftheriades, Binary Huygens' metasurfaces: Experimental demonstration of simple and efficient near-grazing retroreflectors for TE and TM polarizations, *IEEE Trans. Antennas Propag.* **66**, 2892 (2018).
- [25] Y. Jia, J. Wang, J. Yang, Y. Li, Y. Pang, Y. Fan, S. Sui, and S. Qu, Wideband planar retro-reflective metasurfaces for backscattering enhancement under oblique incidence, *J. Phys. D: Appl. Phys.* **51**, 335103 (2018).
- [26] X. Wang, A. Díaz-Rubio, V. S. Asadchy, G. Ptitsyn, A. A. Generalov, J. Ala-Laurinaho, and S. A. Tretyakov, Extreme

- Asymmetry in Metasurfaces Via Evanescent Fields Engineering: Angular-Asymmetric Absorption, *Phys. Rev. Lett.* **121**, 256802 (2018).
- [27] Q. Wang, L. Zhou, P. Wan, D. Huang, H. Guo, Y. Ren, X. Cao, and J. Du, Retroreflection from a single layer of electromagnetic Helmholtz cavities based on magnetic symmetric dipole modes, *Opt. Express* **28**, 30606 (2020).
- [28] Y.-Q. Liu, S. Li, J. Guo, L. Li, and H. Yin, Planar microwave retroreflector based on transmissive gradient index metasurface, *New J. Phys.* **22**, 063044 (2020).
- [29] A. Díaz-Rubio and S. Tretyakov, Dual-Physics Metasurfaces for Simultaneous Manipulations of Acoustic and Electromagnetic Waves, *Phys. Rev. Appl.* **14**, 014076 (2020).
- [30] S. Tretyakov, *Analytical Modeling in Applied Electromagnetics* (Artech House, Boston, 2003).
- [31] S. Tretyakov, V. Asadchy, and A. Díaz-Rubio, Metasurfaces for general control of reflection and transmission, in *World Scientific Handbook of Metamaterials and Plasmonics* (World Scientific, Singapore, 2017), pp. 249–293.
- [32] P. Christian, Retroreflective binary Huygens' metasurface, Master's thesis, University of Toronto, 2018.
- [33] C. Shen, A. Díaz-Rubio, J. Li, and S. A. Cummer, A surface impedance-based three-channel acoustic metasurface retroreflector, *Appl. Phys. Lett.* **112**, 183503 (2018).
- [34] D. M. Pozar, *Microwave Engineering*, 3rd ed. (Wiley, New York, 2004).
- [35] X. Wang, A. Díaz-Rubio, A. Sneek, A. Alastalo, T. Mäkelä, J. Ala-Laurinaho, J.-F. Zheng, A. V. Räsänen, and S. A. Tretyakov, Systematic design of printable metasurfaces: Validation through reverse-offset printed millimeter-wave absorbers, *IEEE Trans. Antennas Propag.* **66**, 1340 (2018).